IEEE Access
Multidisciplinary | Rapid Review | Open Access Journal

Received 8 December 2023, accepted 25 December 2023, date of publication 11 January 2024, date of current version 24 January 2024.

Digital Object Identifier 10.1109/ACCESS.2024.3352914

RESEARCH ARTICLE

On the Relative Effect of Underwater Optical Turbulence in Different Channel Conditions

CALLUM T. GELDARD, JOHN S. THOMPSON, (Fellow, IEEE), AND WASIU O. POPOOLA
School of Engineering, Institute for Imaging Data and Communications, The University of Edinburgh, EH9 3JL Edinburgh, U.K.

Corresponding author: Callum T. Geldard (cgeldard@ed.ac.uk)

This work was supported by EPSRC under Grant EP/X04047X/1.

ABSTRACT This paper presents a simulation framework for modelling optical underwater turbulence in conjunction with absorption and scattering. Using this technique, the channel is evaluated in two ways: the turbulent statistics in different channel conditions; and the stationary channel characteristics. The turbulent statistics observed from the simulation show that the relative impact of turbulence on a received signal is lower in a highly scattering channel, showing an in-built resilience of these channels. Received intensity distributions are presented, showing that the commonly used Log-Normal fading model provides a good description of the fluctuations in received optical power due to the effect of turbulence. When considering stationary channel characteristics, the effect of turbulence induced scattering is shown to cause and increase both spatial and temporal spreading at the receiver plane. The impact of turbulence - as measured using this new modelling framework - on the channel capacity is equally investigated to provide context to the implications of the channel modelling findings on underwater optical wireless communications link performance.

INDEX TERMS Channel models, free-space optical communication, multipath channels, photonics, underwater communication.

I. INTRODUCTION

Underwater optical wireless communications (UOWC) is an application in the field of optical wireless communications (OWC) that could complement the traditional acoustic method of transmission. Some of the inherent advantages of UOWC over the dominant acoustic underwater communications technology include lower latency and higher data rate [1]. These advantages, coupled with the lower transmission power associated with the semiconductor devices used in OWC, can enable remote high speed wireless communication over tens of metres. The removal of cables, typically used for high speed communications, could save time and money for ships in a harbour and for remotely operated vehicles (ROV) or for retrieving data from sensor nodes in coastal water or the open sea.

Designing an efficient optical wireless communications system for the underwater environment requires a detailed knowledge of the channel and an understanding of how these different types of water affect signal transmission. This channel knowledge is useful when determining the required link margin when developing a UOWC link for a given application as well as when choosing what signalling techniques may be required for optimal performance. Measuring channel characteristics can be expensive and in some cases impractical. So, simulation is invaluable for gaining channel knowledge when designing a communications system for a constantly changing environment such as the turbulent UOWC channel.

The paper is structured as follows, the contributions of this work are placed in the context of existing studies in Section II. Then Section III provides some background information on the theory that underpins the work detailed within this paper, Section IV describes the simulation framework, and Section V discusses the method of estimating the channel capacity. In Section VI, we present the results and discuss their significance, and in Section VII, we draw our final conclusions.

II. EXISTING WORK AND CONTRIBUTIONS

Based on the principle of radiative transfer theory, previous studies in the literature have detailed methods for simulating the absorption and scattering effects of the UOWC channel model as in [2], [3], [4], [5], and [6]. Other studies have

The associate editor coordinating the review of this manuscript and approving it for publication was Sukhdev Roy.

investigated turbulence in simulation as a separate entity including [7], and these results have been confirmed through experimental work in [8]. All of these references utilise a form of photon tracking Monte-Carlo (MC) simulation to model photon propagation through the underwater channel. Recent works have attempted to combine these two channel phenomena (turbulence and scattering/absorption effects) in simulation, including [9], [10], [11], and [12] and our earlier works [13], [14]. The works reported in [9] and [10] utilised phase screens to model turbulence in combination with a photon tracking simulation to model particulate scattering with their results presented in terms of average channel gain and channel impulse response (CIR). In addition to this, reference [10] presented the received intensity distributions under certain channel conditions.

Rather than simulating turbulence with phase screens on-top of scattering from particles, some papers have attempted to build a truly holistic channel modelling simulation where scattering from particles and turbulence are considered in the same process. In [11] the authors consider a turbulence induced scattering model based on a theoretical oceanic refractive index spectrum to evaluate the average path loss, CIR, and received intensity distributions in clear and coastal waters. In [12] the CIR and attenuation coefficients using a composite scattering model for different water conditions are investigated for a range of bubble populations. Finally, our prior works in [13], [14], and [15] explore the stationary channel characteristics of a UOWC in the presence of turbulence induced scattering using the photon tracking MC simulation used in this paper. All of these works show that when turbulence is considered, the received optical power is reduced and the temporal distribution of the CIR is increased. Furthermore, the framework presented in this paper has been used to study the turbulent characteristics of the UOWC channel in thesis [15]. The results indicate that the composition of the UOWC channel has an affect on the impact of turbulence on the received signal.

Turbulence is considered extensively in UOWC literature. However, when evaluating link performance, it is common to consider only the effects of turbulence at the receiver as a fading phenomena, as in [16], [17], [18], [19], [20], [21], and [22]. This method models the effects of the turbulence on the received signal rather than the underlying process itself. This way of considering turbulence is borrowed from terrestrial OWC where scattering is not a major consideration which is not always the case in UOWC. Whilst this technique is valid for comparing the performance of different modulation and signal processing techniques under turbulent conditions, as it is used in literature, it does not allow for an investigation into the relative impact of turbulence in different levels of turbidity, as is the aim of this study.

The main contribution of this paper is to present a comprehensive modelling approach that accounts for turbulence alongside absorption and scattering in a single model. Through the use of this new modelling technique, we examine through simulation the relative impact of turbulence in different water conditions for the first time in literature - this is only possible due to the new model. Finally, the previously evaluated links are compared in terms of their data transmission performance. This allows us to show how the communication performance is affected by changes in water type and turbulence strength.

III. BACKGROUND

A. ABSORPTION AND SCATTERING

When photons propagate through water, they are subject to scattering and absorption dependent upon the composition and condition of the water medium [1]. The probability of a single scattering or absorbing interaction as a photon travels through space is described by the absorption and scattering coefficients, denoted by $a(\lambda)$ and $b(\lambda)$ respectively, with λ denoting the wavelength dependency of the coefficients. The combined likelihood of any interaction taking place is therefore given by the extinction coefficient $c(\lambda)$ given by [2]:

$$c(\lambda) = a(\lambda) + b(\lambda). \tag{1}$$

For simplicity throughout the rest of this paper when describing these coefficients, λ will be omitted from the notations but it should be understood that these quantities are wavelength dependent. A higher c means a photon is more likely to undergo a scattering or absorption event. Absorption occurs when a photon-particle interaction causes a photon to lose all of its energy and therefore stop propagating. Its effect on received signal power is entirely attenuating. Elastic scattering is of particular interest as it occurs when a photon-particle interaction results in a change of the photon's propagation path. This change in direction can be observed at the receiver (Rx) as attenuation but also as dispersion in both time and space due to multipath propagation [5], [14]. These coefficients have been evaluated through experimental studies, most notably by Petzold in [23].

The derivation of a and b from experimental measurements is outlined in [23] and [24]. The absorption coefficient, a, can be found by measuring the numbers of photons present at the Rx plane when a known number are transmitted through a small body of water. Conversely, the measurement of the scattering coefficient, b, requires the measurement of the volume scattering function (VSF), $\beta(\theta)$, which dictates the probability of a photon being scattered at a certain angle. This process involves moving an Rx around a point and measuring the number of photons incident at each angle of displacement. When $\beta(\theta)$ is integrated over all possible angles the likelihood of a single scattering interaction becomes [2]:

$$b = 2\pi \int_0^{\pi} \beta(\theta) \sin(\theta) d\theta. \tag{2}$$

B. TURBULENCE

An additional component of the UOWC channel is turbulence. Turbulence in water is caused by fluctuations in the refractive index which arise from random variations in

salinity and temperature [25]. When a photon propagates through the turbulent UOWC channel, these 'pockets' with different refractive indices cause an alteration in direction. At the Rx this may be realised in the form of fluctuations in received power. This variation in power is described by the scintillation index, defined as [1]:

$$\sigma_I^2 = \frac{\langle I^2 \rangle - \langle I \rangle^2}{\langle I \rangle^2}, \tag{3}$$

where I is the received intensity and $\langle . \rangle$ denotes the ensemble average. It may be useful when designing an UOWC link to have a closed form expression for σ_I^2 in water conditions expected for the location that the link will operate in. This would have to take the form:

$$\sigma_I^2 = f(T, S, a, b, Z_{link}, \ldots), \tag{4}$$

where $f(.)$ denotes a function of temperature, T; and salinity, S; as well as the transmission length, Z_{link}; absorption; and scattering coefficients, and any other channel parameter. However, to the best of the authors knowledge no such expression exists in literature. Although analytical studies have explored the impact of various link conditions in pure water, i.e. ignoring absorption and scattering parameters, including in [26], [27], and [28]. These findings suggest that an increase in T, S, or Z_{link} cause an increase the effect of turbulence on the optical signal.

C. TURBULENCE INDUCED SCATTERING

If an expression that satisfies (4) exists then it cannot be found unless absorption, scattering, and turbulence are brought together in a single simulation. Scattering is defined for the purposes of channel modelling as any interaction that causes a photon to change direction [24]. Therefore, the refraction caused by turbulence can be modelled in the same way as a photon-particle interaction in simulation as both are scattering events. Furthermore, the VSF of temperature induced turbulence and bubble induced turbulence have been empirically observed in [29] and [30], respectively. Scattering due to temperature induced turbulence was found to be heavily weighted towards scattering angles below 1^o [29]. This small angle scattering was also briefly discussed in [25] but has been omitted from literature in part due to the misconception that scattering at very small angles is analogous to no scattering at all as in [31]. However, the focus of these works was solar irradiance rather than laser emitted photons as in UOWC. Here, when multiple scattering is considered, the cumulative effects of small angle scattering will be borne out at the Rx plane. Including changes to the spatial and temporal distributions of the photon beam when compared to the case with no turbulence induced scattering.

For modelling purposes, the scattering coefficient can be split into its constituent parts to allow their contributions to be examined separately [24]. Throughout this paper, subscripts sw, p, and t will be used to denote the scattering contributions from seawater, particles, and turbulence respectively. Thus:

$$b = b_{sw} + b_p + b_t. \tag{5}$$

When Petzold measured the commonly used values of b in certain water types the accuracy was limited by a sensitivity of 0.1^o [23]. Therefore, commonly used b values do not include the smallest angle scattering - which in a turbulent channel is the most common. As such, in order to account for turbulence induced scattering accurately, expression (5) should be revised to show Petzold's value with the addition of an adjustment term. That is:

$$b = b_{Petzold} + b_t. \tag{6}$$

As integration is a linear operation, the total VSF of any water channel - which is linked to b in (2) - can also be split into its constituent parts. Then it can be represented by the sum of each component's VSF weighted by its scattering coefficient. That is:

$$b\beta(\theta) = b_{sw}\beta_{sw}(\theta) + b_p\beta_p(\theta) + b_t\beta_t(\theta). \tag{7}$$

This simplifies the generation of the VSF in computation by allowing individual functions to be used to represent each component of the channel. Then in simulation, when a photon undergoes a scattering interaction the likelihood of it being due to seawater, particles, or turbulence is built into the VSF of the channel. In this paper, the VSF of seawater and particle induced scattering are represented by Mie scattering and a Henyey-Greenstein (HG) function respectively as in literature [1], [24], [25]:

$$\beta_{sw}(\theta) = 0.06225(1 + 0.835\cos(\theta)^2) \tag{8}$$

$$\beta_p(\theta) = \frac{1 - g^2}{4\pi\left(1 + g^2 - 2g\cos(\theta)\right)}, \tag{9}$$

for all water conditions $\beta_p(\theta)$ is modelled with an average cosine, g, equal to 0.975. This value of g was selected based on the need to optimise $\beta_p(\theta)$ for the larger angle scattering and the findings in [3] that suggest the commonly used $g = 0.924$ understates scattering at angles greater than 100^o. The newly introduced turbulence induced scattering is modelled through the Fournier-Forand (FF) function [32]. This function was originally proposed to better model particulate scattering in the ocean, especially at small angles. In this work, the FF function is repurposed to model turbulence induced scattering. It is selected for this framework as the function links $\beta_t(\theta)$ to the refractive index of water and is highly weighted towards small angles. It is given as:

$$\begin{aligned}\beta_t(\theta) = \frac{1}{4\pi(1-\delta)^2\delta^v}&[v(1-\delta) \\ &- (1-\delta^v) + [\delta(1-\delta^v) \\ &- v(1-\delta)]\sin^{-2}\left(\frac{\theta}{2}\right)] \\ &+ \frac{1-\delta_{180}^v}{16\pi(\delta_{180}^v - 1)\delta_{180}^v}(3\cos^2\theta - 1),\end{aligned} \tag{10}$$

where, $v = \frac{3-m}{2}$ with $m = 3.05$ being the Junge slope parameter. Also δ is defined as:

$$\delta = \frac{4}{3}(n-1)^{-2}\sin\left(\frac{\theta}{2}\right)^2, \tag{11}$$

where n is the refractive index of water and δ_{180} is expression (11) evaluated at $\theta = 180^{o}$. Using the FF function and (2) the value of b_t can be linked directly to n, as shown in Fig. 1. When n is close to 1, a small increase yields a large corresponding increase in b_t. This rate of change then decreases when n is greater than 1.5 and b_t approaches an asymptote at approximately 0.53 m^{-1}. However, these more optically dense refractive indices are not realistic for water and used for illustrative purposes only.

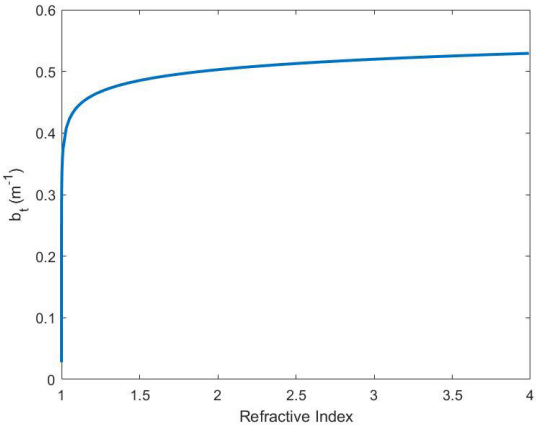

FIGURE 1. The turbulence induced scattering coefficient, b_t, obtained using the proposed FF VSF function in conjunction with (2) plotted against refractive index, n.

It should be further noted that it would be nearly impossible to define a $\beta_t(\theta)$ that fits with any measured values due to the random nature of turbulence and all the factors that would affect it. The purpose of this work is not to find an exact channel model that works in all conditions but is to show the relative impact of different parameters on link performance, thus the qualitative results from the simulation are of more interest than the quantitative results. As such, in the following simulation n is fixed to 1.33 with a normalised $\beta_t(\theta)$ used for all b_t. The effect of turbulence induced scattering is then represented by a changing b_t, similarly to the way the HG function is used to model particulate scattering in [3]. This reduces the computational complexity of the simulation by allowing a single look-up table be used for $\beta_t(\theta)$ in all turbulent conditions, rather than recalculating (10) when b_t changes. If the simulation were to be used to model a specific type of turbulence (i.e. temperature, salinity, or bubble induced turbulence) then the FF could be replaced with a more appropriate VSF based on empirical measurements, such as that for bubbles from [30]. However, these measurements will not always be general to all waters so results obtained using a specific VSF could be limited to certain channel conditions.

IV. SIMULATION FRAMEWORK

This section describes the simulation framework proposed to incorporate turbulence induced scattering into the UOWC channel model. The basis for this framework is a photon tracking Monte-Carlo (MC) simulation similar to those used in literature, including [2], [3], [4], [5], and [6]. Here, the propagation of N photon packets are tracked as they traverse the UOWC channel. The photon propagation is dictated by the absorption and scattering properties of the channel. Using (5)-(11), the VSF for each constituent scattering component is considered along with the absorption coefficients, taken from Petzold's coastal and harbour water case studies. The effect of turbulence induced scattering, as introduced in section III-C, is investigated in different water conditions by repeating the the photon tracking simulation a number of times with a changing b_t to represent fluctuations in the channel due to turbulence. In this framework, b_t may take any value between $[0, b_{t_{max}}]$. Hence a uniform distribution is selected such that all values within the range are equally likely to occur during the simulation. Thus, the turbulent channel is modelled as a series of stationary channels with a random b_t. This is based on the assumption that the channel propagation time is much lower than its coherence time, following results presented in [33] which show the minimum coherence time of a 30 m link to be around 10^{-5} s. The weighted sum of all photons received for each iteration are used to calculate σ_I^2 using (3) and plotted as a histogram. The histogram is normalised to obtain a probability density function (pdf) of the distribution of received photon intensities.

The effect turbulence induced scattering has on the stationary channel characteristics is then explored by considering the temporal and spatial dispersion for a fixed value of b_t. This provides a deeper understanding of how turbulence induced scattering affects the received signal in UOWC. The received on-axis channel impulse response (CIR) obtained through the MC simulation is then fitted with the double-Gamma function (DGF) shown in (12), this was first proposed for light propagation through clouds in [34] and subsequently applied to the UOWC channel in [4]. The DGF provides a simple, parameterised, mathematical representation of the CIR. Using this, the frequency response of the channel may be obtained by taking the Fourier transform of the DGF, as shown inset in Fig. 2. A further benefit of the DGF is that it provides a computationally simple method of storing the CIR for future channel analysis. Whereby the DGF fitting coefficients, C_i, $i = 1, 2, 3, 4$, rather than saving the output of the MC simulation or re-running the simulation each time which are both resource intensive.

$$h(t) = C_1 t \exp(-C_2 t) + C_3 t \exp(-C_4 t) \tag{12}$$

The photon tracking MC simulation and DGF are validated prior to further analysis using a 15 m harbour link with $b_t = 0$ m^{-1} for illustrative purposes. Fig. 2 shows the DGF fitted to the simulation data for two different realisations of the same 15 m harbour link with $b_t = 0$ m^{-1}. The DGF curve is shown to provide a good fit to the data clouds obtained via the MC simulation. As evidenced by the coefficient of determination, R^2, being greater than 0.95 for the channel realisations with 10^9 and 10^{10} photon packets. With the impulse responses from the realisations of the photon tracking simulation displaying convergence around

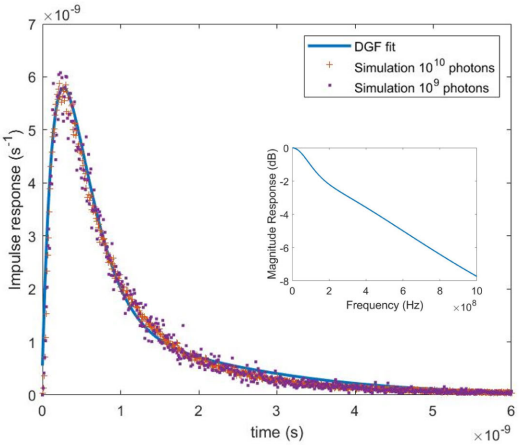

FIGURE 2. Impulse response of a 15 m harbour water link, with $b_t = 0$ m^{-1}, from MC simulation run with both 10^{10} and 10^9 photons fitted to the DGF with frequency response inset.

the trend described by the DGF. This convergence, even for a relatively low number of simulated photon packets, relative to the channel gain, is due to the weighting factor used in the simulation that accounts for the likelihood of a photon reaching the Rx. This means that fewer photons need be simulated than if the received photons were simply counted [24]. Thus, reducing the computational requirements of the running the photon tracking simulation. This is especially useful when the CIR itself is not of interest, as is the case for the investigation into the relative effect of turbulence in different water conditions.

V. CHANNEL CAPACITY

Next, the previously characterised channels are used to model data transmission in UOWC. Here, the DGF fitted to the on-axis CIR is used to compare the link capacity in different turbulence conditions. For a UOWC system using intensity modulation with direct detection (IM/DD), the time continuous received signal is given by [35]:

$$y(t) = P_{\mathrm{t}} R_e x(t) * h(t) + n(t) \tag{13}$$

where P_{t} is the transmitted power, R_e is the responsivity of the photodetector (PD), and $n(t)$ is additive white Gaussian noise (AWGN). When the channel contains a temporally dispersive component, as in this study, the effect is represented by the convolution of the transmitted signal, $x(t)$, and the CIR, $h(t)$, denoted by the convolution operator, $*$. In a turbulent link $h(t)$ would vary as the channel composition fluctuates. The coherence time of a UOWC link describes the shortest time for which the channel is stable. This has been evaluated analytically in [33], where it was shown to be orders of magnitude greater than the transmission duration of Gbps communications. Therefore, assuming accurate channel state information can be gathered during transmission, the limiting factor will be the temporal spread in $h(t)$. Resultantly, the channel capacity is compared at $b_{t_{max}}$ for each turbulence condition, as this will be the point with the worst performance. Thus, causing a bottle neck in the link capacity.

The capacity of an ideal filter channel, C_{ideal}, where the frequency response is flat for the whole bandwidth, B, is given by [36]:

$$C_{ideal} = B \log_2 (1 + \gamma) . \tag{14}$$

where, $\gamma = \frac{P_{\mathrm{t}}^2 R_e^2 H_0^2 \sigma_x^2}{\sigma_n^2}$ is the signal to noise ratio (SNR) with H_0; σ_x^2; and σ_n^2 denoting the total channel gain; the variance in the data signal; and the noise variance, respectively.

However, practical UOWC channels, including those described by the DGF have an SNR imbalance across the frequency response, as shown inset in Fig. 2. Here, the temporal dispersion caused by multiple scattering means the frequency response is not flat within the bandwidth. The average capacity of a non-ideal filter channel can then be found by splitting the signal bandwidth into N blocks of bandwidth Δf, as in [36]:

$$C_{non-ideal} = \Delta f \sum_{i}^{N} \log_2 (1 + \gamma_i). \tag{15}$$

If Δf is suitably small, then the frequency response within each subcarrier band should be flat and $\gamma_i = \frac{P_{\mathrm{t}}^2 R_e^2 H_i^2 \sigma_{x_i}^2}{\sigma_{n_i}^2}$ where H_i; $\sigma_{x_i}^2$; and $\sigma_{n_i}^2$ denoting the channel gain; the variance in the data signal; and the noise variance, of the i^{th} subcarrier respectively. Equation (15) is solved by estimating the γ_i from the error vector magnitude of a known pilot sequence, as in [37].

VI. UOWC CHANNEL SIMULATION RESULTS

This section presents results obtained using the aforementioned simulation framework. The turbulent nature of the UOWC channel is first investigated in a range of link conditions. Following this, the stationary channel is examined to gain a deeper understanding of the effect of turbulence induced scattering on photon propagation in terms of temporal and spatial dispersion.

A. TURBULENT CHANNEL SIMULATION

The random effect of b_t on the received photon intensity is investigated by transmitting 10^7 photons through the channel, repeated for 1500 Monte-Carlo iterations using the simulation framework described in section IV. The relative effect of turbulence is investigated on three different channels, they are: 15 m coastal water; 30 m coastal water; and 15 m harbour water. These channels were selected to allow the impact of water type and link distance to be observed.

First, the received intensity distributions of the stationary channel, with fixed b_t, are investigated to confirm that the results obtained from the photon tracking simulation are repeatable and therefore useful for use within the proposed framework. When $b_{t_{max}} = 0$ m^{-1}, i.e. no turbulence, the

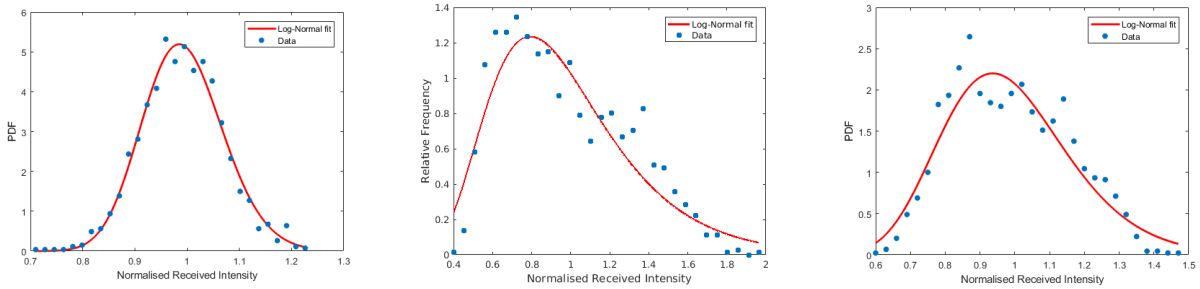

(a) 30 m coastal link, $b_{t_{max}} = 0$ m^{-1}

(b) 30 m coastal link, $b_{t_{max}} = 0.05$ m^{-1}

(c) 15 m harbour link, $b_{t_{max}} = 0.5$ m^{-1}

FIGURE 3. Log-Normal pdf fits on histograms showing variation in received photon counts at the Rx for selected channel conditions. The relevant fit parameters can be found in Table 2.

intensity distributions across all three links have a Gaussian shape with normalised mean of approximately 1 with the received distribution for the 30 m coastal link shown in Fig. 3a. In Table 1 the R^2 values for all three distributions is shown to be very close to 1. Indicating that the Gaussian distribution provides a very good fit, as would be expected for a link with no turbulence. The normalised variance in the received intensities, denoted by σ^2 in Table 1, are expectantly small for all channels considered. This variance is due to the random nature of scattering modelled in the photon tracking MC simulation. The fact that σ^2 is small and the mean is approximately 1 shows that the total received intensity from the simulation converges for a single value of b_t.

TABLE 1. Gaussian fit parameters for the three channel conditions with no turbulence.

	σ^2	mean	R^2
Coast 15 m	1.83×10^{-5}	0.9996	0.99
Coast 30 m	0.0059	0.9896	0.98
Harbour 15 m	0.0042	0.9933	0.98

Next, the turbulence properties of the channel are investigated by varying the b_t in line with the proposed simulation framework. A Log-Normal function is fitted to the received intensity distributions obtained using the simulation. The histograms and respective fits of some selected channel realisations are shown in Fig. 3. The mean normalised variance of the simulation and fitted Log-Normal scintillation index, σ_I^2 and σ_{Log}^2 respectively, as well as the mean log intensity, μ, for these fits are given in Table 2. The Log-Normal model of turbulence gives a reasonably good fit for the distributions with $R^2 > 0.75$ for all cases. This is inline with the expectation that when turbulence is present in the channel, the received intensity distribution becomes non-Gaussian in shape.

In order to compare relative impact of turbulence induced scattering for different UOWC channels, σ_I^2 is plotted against $b_{t_{max}}$ in Fig. 4. When comparing between channel configurations it is apparent that the relative impact of turbulence induced scattering is lessened when there are already a high number of scattering interactions per channel. In Fig. 4 it is clear that increasing the link distance for coastal

TABLE 2. Simulation and Log-Normal fit parameters for simulation of turbulent harbour and coastal UOWC channels with link rages of 15 and 30 m.

$b_{t_{max}}$ (m^{-1})	σ_I^2	σ_{Log}^2	μ	R^2
15 m, Coastal Water				
0	1.84×10^{-5}	1.84×10^{-5}	-9.21×10^{-5}	0.98
0.2	0.3202	0.5297	-0.3312	0.80
0.3	0.6399	0.8958	-0.7696	0.90
30 m, Coastal Water				
0	0.0060	0.0061	0.0091	0.98
0.01	0.0105	0.0113	-0.0110	0.98
0.05	0.1001	0.1437	-0.0887	0.87
0.1	0.3204	0.4273	-0.2671	0.83
0.15	0.5828	0.6999	-0.4810	0.88
0.2	1.0374	2.0862	-0.9923	0.82
15 m, Harbour Water				
0	0.0044	0.0042	-0.0055	0.98
0.5	0.0271	0.0362	-0.0295	0.89
1	0.0792	0.1087	-0.0846	0.82
2	0.2389	0.3279	-0.2238	0.79
5	0.8763	1.5284	-0.7106	0.98

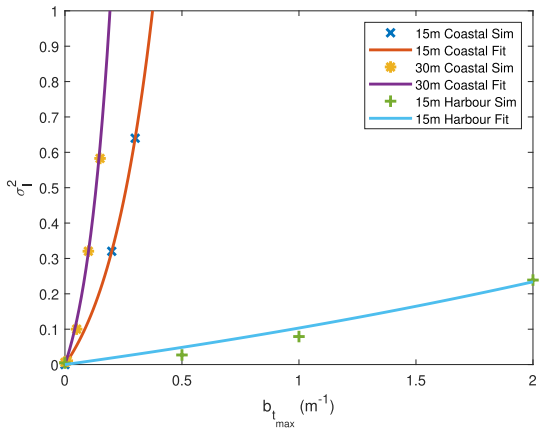

FIGURE 4. σ_I^2 vs $b_{t_{max}}$ in different water types and link ranges.

water yields an increase in σ_I^2 for the same $b_{t_{max}}$. For example when $b_{t_{max}} = 0.2$ m^{-1}, $\sigma_I^2 = 0.3202$ for a link distance of 15 m compared to 1.0374 when $Z_{link} = 30$ m. This is in line with the Z_{Link} dependency of the expression derived in reference [26]. However it is when comparing between the 15 m coastal and harbour links that the results deviate from when absorption and scattering are omitted. In the harbour channel a $b_{t_{max}}$ greater than 1 m^{-1} is required to yield a

$\sigma_I^2 > 0.1$ compared to $b_{t_{max}} = 0.1$ m^{-1} in coastal water over the same link range. Referring to Fig. 1, values of $b_t > 0.5$ m^{-1} are not realistic as the n would be beyond what is possible for water. Meaning that in reality, turbulence will have less of an effect in a highly turbid harbour channel, than in clear coastal waters. This supports the suggestion that, due to the multiple scattering nature of the UOWC channel, it is not accurate to simply adapt concepts from free space optics (FSO) to the underwater channel.

B. STATIONARY CHANNEL CHARACTERISTICS

The characteristics of the stationary channel are next investigated to gain an understanding of why the effect of turbulence induced scattering is lessened in a channel that already has a high degree of scattering. For this part of the study, the photon tracking MC simulation is run with 10^9 photons to ensure the convergence of the temporal and spatial response for further analysis.

1) PHOTON TEMPORAL DISTRIBUTION

The CIR in Fig. 2 illustrates the temporal response of the UOWC channel in harbour water with no turbulence. The temporal spread due to multiple scattering can further be quantified in terms of the root mean delay spread, D_{rms}. In this work, the D_{rms} is used to further validate the agreement between the MC simulation and DGF model, as well as allowing for a comparison between the temporal response of the different channel conditions under test.

The D_{rms} of the simulation is denoted by D_{rms}^{sim}, whilst that of the DGF fit is D_{rms}^{DGF}. Both D_{rms} are plotted against b_t in Fig. 5 and D_{rms}^{DGF} is shown to be close to the corresponding D_{rms}^{sim} for all channel conditions simulated. The DGF coefficients, C_i, for channel conditions used later in this paper are presented along with the respective R^2 in Table 3. The R^2 value for each fit is greater than 0.9 which indicates the DGF model describes MC data set adequately for all parameters used. This justifies the use of the DGF fits rather than raw simulation data in the rest of the paper.

TABLE 3. Fit parameters for DGF for the coastal and harbour channels with $\phi_{Tx} = 1.5$ mrad and $FOV = 10^o$ at different values of b_t when the CIR is sampled at a rate of 10 Gsam/s.

b_t (m^{-1})	C_1	C_2	C_3	C_4	R^2
30 m, Coastal Water					
0	2×10^6	1.15×10^{11}	4072	1.2×10^{10}	1.00
0.05	5.5×10^5	1×10^{11}	2544	1×10^{10}	1.00
0.1	1.86×10^5	9×10^{10}	2953	1.2×10^{10}	1.00
0.2	1.2×10^4	3×10^{10}	435	6×10^9	0.90
15 m, Harbour Water					
0	600	3.8×10^9	28.49	9×10^8	0.97
0.5	160	3.0×10^9	23.69	9×10^8	0.99
1	60	2.4×10^9	12.51	7.5×10^8	0.97
2	8.9	1.2×10^9	2.40	4.5×10^8	0.95

Fig. 5a and 5b show D_{rms} against b_t for a 30 m coastal link and 15 m harbour link respectively with different Tx and Rx configurations. The D_{rms} of the 15 m harbour water link with $b_t = 0$ m^{-1} is more than 10 times greater than that of the 30 m coastal channel with no turbulence, meaning the harbour channel is the more dispersive of the two channels. This difference in temporal dispersion means that the two channel conditions respond differently to changes in Tx and Rx configuration. Whilst the Rx FOV has no impact on D_{rms} in either channel, a larger Tx divergence angle (ϕ_{Tx}) in the coastal channel causes the D_{rms} to increase. Conversely, in the more highly scattering harbour channel there is no clear change in D_{rms} due to a change in ϕ_{Tx}, as the impact of the channel is greater than that of the link geometry.

This difference in the impact due to link geometry highlights the effect multiple scattering has on a channel. Further to this, the addition of turbulence induced scattering has a different effect on D_{rms} in the already highly scattering harbour water compared to the coastal water link. The values of b_t used in Fig. 5a are 10 times smaller than those in Fig. 5b however the increase in D_{rms}^{DGF} compared to when $b_t = 0$ m^{-1} is larger. For the case of $b_t = 0.1$ m^{-1} in coastal water D_{rms}^{DGF} is 5.81 times larger than $b_t = 0$ m^{-1}. Whereas for $b_t = 1$ m^{-1} in harbour water it is only 1.78 times larger. This again implies that a channel that already has a high level of multiple scattering possesses a higher level of tolerance to turbulence induced scattering. From a communications perspective this increase in temporal dispersion will cause the energy of a transmitted symbol to spread out leading to ISI in the received signal. Due to the lack of any significant impact on D_{rms} due to FOV and ϕ_{Tx} in harbour waters the rest of this paper will follow using an FOV of 10^o and $\phi_{Tx} = 1.5$ mrad as a case study across all water conditions.

2) PHOTON SPATIAL DISTRIBUTION

Next, the spatial distribution at the receiver plane is investigated. Shown in Fig. 6 are the 2-dimensional Rx plane intensity distributions in both coastal and harbour waters at different values of b_t. When comparing the spatial distributions for $b_t = 0$ m^{-1} it is noticeable that for the case of highly scattering harbour water, the intensity is scattered over a much greater area in the Rx plane. In fact the full width half maximum (FWHM) beamwidth is approximately 5.5 m whereas for coastal water it is 1.1 m. These figures are in line with the expectation of more photon-particle interactions due to the longer scattering length, bZ_{link}, of the harbour link. The extinction length in a 15 m harbour channel is approximately 28 interactions, compared to 7 for a coastal channel of $L = 30$ m. For both water types this FWHM beamwidth increases as b_t increases, however the magnitude of its contribution is different for each water type, expectantly.

Further evidence of a difference in the relative impact of turbulence induced scattering can be found when comparing the channel gains in different channel conditions. For the case of the highly scattering 15 m harbour channel in Fig. 6, the channel gain at perfect alignment (i.e. Spatial Offset = 0 m) is 7.72×10^{-7} when $b_t = 0$ m^{-1} and it decreases by 59% when b_t increases to 1 m^{-1}. Comparatively, in the 30 m coastal channel the aligned channel gain for $b_t = 0$ is 2.02×10^{-6} and it falls by 44% when $b_t = 0.05$ m^{-1}, and 63% when $b_t = 0.1$ m^{-1}. This can be explained by

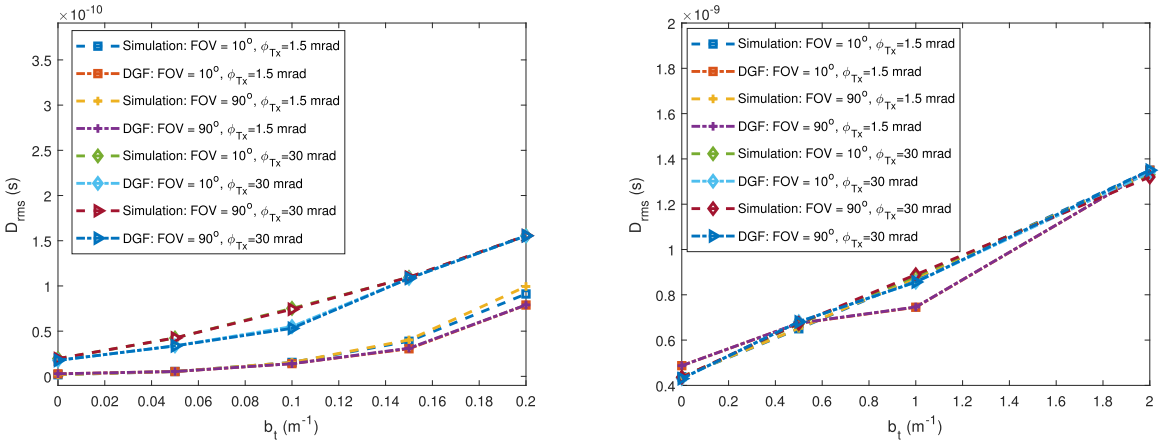

(a) 30 m coastal water link.

(b) 15 m harbour water link.

FIGURE 5. D_{rms} vs b_t for different UOWC links highlighting the relative impact of turbulence induced scattering on temporal dispersion.

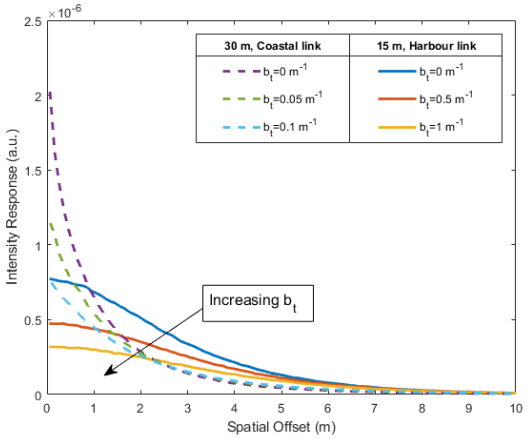

FIGURE 6. Rx plane spatial intensity distribution for 30 m coastal, and 15 m harbour water link with different conditions of turbulence induced scattering.

returning to the definition of turbulence induced scattering as being a case of small angle scattering. When the number of scattering interactions per channel is high then the photons are already dispersive and therefore have some resilience to additional scattering at small angles. However, when the number of interactions per channel is lower, as is the case with the 30 m coastal link, the increase can have a much greater impact on the propagation path taken by a photon. Meaning that proportionally turbulence induced scattering has a lesser effect in a channel that already has a high probability of scattering compared to one that does not.

C. RELATIONSHIP TO SCINTILLATION INDEX

As previously stated, an expression for σ_I^2 for given channel characteristics would be useful for link design in UOWC. A fully parameterised expression to satisfy equation (4) will require further investigation. However, based on the results in sections VI-A and VI-B we present an expression to link σ_I^2 to $b_{t_{max}}$ and Z_{link}. An exponential function is fitted to the σ_I^2 values found through simulation, the resulting curves are shown in Fig. 4. The exponential function takes the form:

$$\sigma_I^2 = A_1 \left(\exp\left(A_2 b_{t_{max}} Z_{link}\right) - 1\right), \tag{16}$$

where A_i, $i = 1, 2$, are constants found through least squares curve fitting with the -1 term used to ensure σ_I^2 is non-negative and originates at zero. The constants for each of the three channels shown in Fig. 4 are presented in Table 4 along with the R^2 value for each fit. The R^2 metric of fit is greater than 0.99 for all three channels suggesting the exponential function provides a very good fit for $b_{t_{max}}$ vs σ_I^2 across a range of channel conditions. The values of A_i, $i = 1, 2, 3$, are very similar for the fits of coastal water over both link distances considered. This confirms that σ_I^2 is related to $b_t Z_{link}$ (i.e. the number of turbulence induced scattering interactions per link) rather than simply b_t - and by extension n. It further suggests that, for a given b_t, (16) can be used to evaluate the relationship between link distance and σ_I^2. This expression may be useful for researchers in estimating σ_I^2 in a channel without having to run the full MC simulation framework used in this paper.

TABLE 4. Exponential fitting constants for the curves shown in Fig. 4.

	A_1	A_2	R^2
Coast 15 m	0.1986	0.3201	1.00
Coast 30 m	0.2219	0.2956	1.00
Harbour 15 m	0.3889	0.0157	1.00

D. CHANNEL DATA TRANSMISSION

The capacity of the turbulent UOWC channel is estimated by evaluating (15) through MC simulation with $N = 6400$ repeated for 10^6 frames. In Fig. 7, the channel capacity is plotted against σ_I^2 values calculated using (16). Here, the capacity is evaluated with a signal bandwidth of 250 MHz and 25 GHz for the 15 m harbour and 30 m coastal links, respectively, with normalised received SNR in the absence of temporal dispersion of both 10 dB and 20 dB for each

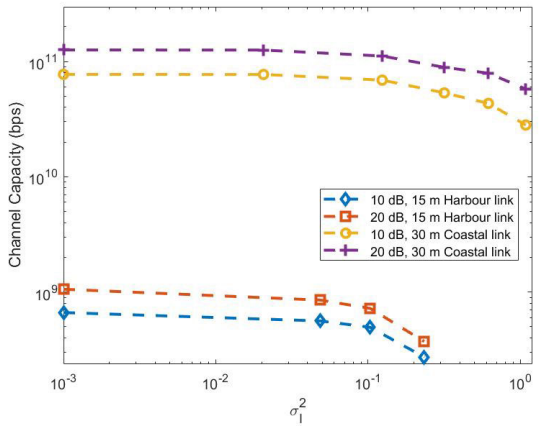

FIGURE 7. Channel capacity vs σ_I^2 for a range of SNR in the 30 m coastal and 15 m harbour water channels.

of the N subcarriers. It can be seen that in both coastal and harbour waters the capacity decreases as σ_I^2 increases, as would be expected given the increased temporal dispersion due to turbulence induced scattering. The effect of this causes distortion in the received time-series signal thereby degrading performance. In a practical system, this would be further compounded by the increased transmitted power requirements due to the turbulence induced fading effect caused by increase spacial dispersion reducing the total channel gain.

The curves in Fig. 7 show that, despite the different $b_{t_{max}}$ required to yield a given σ_I^2, the relative impact of σ_I^2 on the channel capacity is proportionally similar for both channels considered in this case study. The implication of this being that although σ_I^2 has a similar effect in different channel conditions, the higher b_t required to cause those conditions means high turbulence can be considered unlikely in a more turbid channel. As a result, link designers can focus on other, more pressing, issues when planning a UOWC link for harbour water conditions.

Assuming accurate channel state information can be obtained within the channel coherence time, then in coastal water over a 30 m link a maximum data rate of $>$ 100 Gbps can be attained when there is no turbulence. Similarly over a 15 m harbour link data rates approaching Gbps are possible with no turbulence. When turbulence is included in the model then C decreases in both channels and would have to be accounted for with higher link margin and/or channel equalisation. The maximum data rates achieved through these simulations show the potential of UOWC for high data rate transmission over short distances.

VII. CONCLUSION

This paper presents a method of modelling turbulence in the UOWC channel as a scattering component, taking into account different water types rather than assuming generality for all water. The simulation method demonstrates that the impact of turbulence is greater when the channel has a lower number of scattering interactions per link. It is shown that, for a given turbulent stimulus, the σ_I^2 in highly scattering harbour water would be lower than in coastal water. This finding should be considered in future simulation works when modelling system performance in different, turbulent, water conditions. Furthermore, the temporal and spatial impact of turbulence was investigated to give further context for the differences in the relative impact of turbulence induced scattering in different water conditions. It is shown that as turbulence increases, the spatial and temporal spread of the stationary channel also increase, but at different rates for different channel conditions. Finally the maximum data rate achievable in each water type is shown to decrease with an increase in σ_I^2. All these results combined provide evidence that if an UOWC channel is to be accurately modelled then turbulence cannot be examined in isolation from absorption and scattering.

REFERENCES

[1] H. Kaushal and G. Kaddoum, "Underwater optical wireless communication," *IEEE Access*, vol. 4, pp. 1518–1547, 2016.

[2] W. C. Cox Jr., "Simulation, modeling, and design of underwater optical communication systems," Ph.D. dissertation, North Carolina State Univ., 2012. [Online]. Available: https://repository.lib.ncsu.edu/items/330add64-27db-442a-9153-eee7ebe0f9d0

[3] C. Gabriel, M.-A. Khalighi, S. Bourennane, P. Leon, and V. Rigaud, "Monte-Carlo-based channel characterization for underwater optical communication systems," *J. Opt. Commun. Netw.*, vol. 5, no. 1, pp. 1–12, Jan. 2013.

[4] S. Tang, Y. Dong, and X. Zhang, "Impulse response modeling for underwater wireless optical communication links," *IEEE Trans. Commun.*, vol. 62, no. 1, pp. 226–234, Jan. 2014.

[5] A. S. Fletcher, N. D. Hardy, and S. A. Hamilton, "Propagation modeling results for narrow-beam undersea laser communications," *Proc. SPIE*, vol. 9739, pp. 136–147, May 2016, doi: 10.1117/12.2222890.

[6] A. Kammoun, Z. Jiusi, B. S. Ooi, and M.-S. Alouini, "Impact of wavelength on the path-loss of turbid underwater communication systems," in *Proc. IEEE Wireless Commun. Netw. Conf. (WCNC)*, Apr. 2019, pp. 1–7.

[7] Z. Vali, A. Gholami, Z. Ghassemlooy, D. G. Michelson, M. Omoomi, and H. Noori, "Modeling turbulence in underwater wireless optical communications based on Monte Carlo simulation," *J. Opt. Soc. Amer. A, Opt. Image Sci.*, vol. 34, no. 7, pp. 1187–1193, Jul. 2017. [Online]. Available: http://josaa.osa.org/abstract.cfm?URI=josaa-34-7-1187

[8] Z. Vali, A. Gholami, Z. Ghassemlooy, M. Omoomi, and D. G. Michelson, "Experimental study of the turbulence effect on underwater optical wireless communications," *Appl. Opt.*, vol. 57, no. 28, pp. 8314–8319, Oct. 2018.

[9] N. Enghiyad and A. Ghorban Sabbagh, "Impulse response of underwater optical wireless channel in the presence of turbulence, absorption, and scattering employing Monte Carlo simulation," *J. Opt. Soc. Amer. A, Opt. Image Sci.*, vol. 39, no. 1, pp. 115–126, Jan. 2022. [Online]. Available: https://opg.optica.org/josaa/abstract.cfm?URI=josaa-39-1-115

[10] H. Wen, H. Yin, X. Ji, and A. Huang, "Modeling and performance analysis of underwater wireless optical absorption, scattering, and turbulence channels employing Monte Carlo-multiple phase screens," *Appl. Opt.*, vol. 62, no. 26, pp. 6883–6891, Sep. 2023. [Online]. Available: https://opg.optica.org/ao/abstract.cfm?URI=ao-62-26-6883

[11] D. Xu, P. Yue, X. Yi, and J. Liu, "Improvement of a Monte-Carlo-simulation-based turbulence-induced attenuation model for an underwater wireless optical communications channel," *J. Opt. Soc. Amer. A, Opt. Image Sci.*, vol. 39, no. 8, pp. 1330–1342, Aug. 2022. [Online]. Available: https://opg.optica.org/josaa/abstract.cfm?URI=josaa-39-8-1330

[12] L. Kou, J. Zhang, P. Zhang, Y. Yang, and F. He, "Composite channel modeling for underwater optical wireless communication and analysis of multiple scattering characteristics," *Opt. Exp.*, vol. 31, no. 7, pp. 11320–11334, Mar. 2023. [Online]. Available: https://opg.optica.org/oe/abstract.cfm?URI=oe-31-7-11320

[13] C. T. Geldard, J. Thompson, E. Leitgeb, and W. O. Popoola, "Optical wireless underwater channel modelling in the presence of turbulence," in *Proc. IEEE Brit. Irish Conf. Opt. Photon. (BICOP)*, Dec. 2018, pp. 1–4.
[14] C. T. Geldard, J. Thompson, and W. O. Popoola, "A study of spatial and temporal dispersion in turbulent underwater optical wireless channel," in *Proc. 15th Int. Conf. Telecommun. (ConTEL)*, Jul. 2019, pp. 1–5.
[15] C. T. Geldard, "Underwater optical wireless communications in turbulent conditions: From simulation to experimentation," Ph.D. dissertation, School Eng., Univ. Edinburgh, Edinburgh, U.K., 2022.
[16] J. Liu and Y. Dong, "On capacity of underwater optical wireless links under weak oceanic turbulence," in *Proc. OCEANS*, Apr. 2016, pp. 1–4.
[17] F. Akhoundi, A. Minoofar, and J. A. Salehi, "Underwater positioning system based on cellular underwater wireless optical CDMA networks," in *Proc. 26th Wireless Opt. Commun. Conf. (WOCC)*, Apr. 2017, pp. 1–3.
[18] A. Huang, L. Tao, and Q. Jiang, "BER performance of underwater optical wireless MIMO communications with spatial modulation under weak turbulence," in *Proc. OCEANS*, May 2018, pp. 1–5.
[19] Y. Baykal, Y. Ata, and M. C. Gökçe, "Underwater turbulence, its effects on optical wireless communication and imaging: A review," *Opt. Laser Technol.*, vol. 156, Dec. 2022, Art. no. 108624. [Online]. Available: https://www.sciencedirect.com/science/article/pii/S0030399222007721
[20] W. Liu, Z. Xu, and L. Yang, "SIMO detection schemes for underwater optical wireless communication under turbulence," *Photon. Res.*, vol. 3, no. 3, pp. 48–53, Oct. 2015. [Online]. Available: https://opg.optica.org/prj/abstract.cfm?URI=prj-3-3-48
[21] R. Boluda-Ruiz, P. Salcedo-Serrano, B. Castillo-Vázquez, A. García-Zambrana, and J. M. Garrido-Balsells, "Capacity of underwater optical wireless communication systems over salinity-induced oceanic turbulence channels with ISI," *Opt. Exp.*, vol. 29, no. 15, p. 23142, Jul. 2021. [Online]. Available: https://opg.optica.org/oe/abstract.cfm?URI=oe-29-15-23142
[22] S. Han, P. Yue, and X. Yi, "Study of an underwater accurate channel model considering comprehensive misalignment errors," *J. Opt. Soc. Amer. A, Opt. Image Sci.*, vol. 39, no. 6, pp. 1014–1024, Jun. 2022. [Online]. Available: https://opg.optica.org/josaa/abstract.cfm?URI=josaa-39-6-1014
[23] T. J. Petzold, "Volume scattering functions for selected ocean waters," Scripps Inst. Oceanography La Jolla Ca Visibility Lab., San Diego, CA, USA, Tech. Rep. 72-78, 1972.
[24] C. D. Mobley. *Ocean Optics Web Book*. Accessed: Aug. 10, 2021. [Online]. Available: http://www.oceanopticsbook.info/
[25] C. D. Mobley. *Light and Water: Radiative Transfer in Natural Waters*. San Diego, CA, USA: Academic Press, 1994.
[26] O. Korotkova, N. Farwell, and E. Shchepakina, "Light scintillation in oceanic turbulence," *Waves Random Complex Media*, vol. 22, no. 2, pp. 260–266, May 2012.
[27] J.-R. Yao, M. Elamassie, and O. Korotkova, "Spatial power spectrum of natural water turbulence with any average temperature, salinity concentration, and light wavelength," *J. Opt. Soc. Amer. A, Opt. Image Sci.*, vol. 37, no. 10, pp. 1614–1621, Oct. 2020. [Online]. Available: https://opg.optica.org/josaa/abstract.cfm?URI=josaa-37-10-1614
[28] Y. Ata and O. Korotkova, "Wave and phase structure functions of plane and spherical waves in particle-free natural turbulent waters," *Opt. Commun.*, vol. 497, Oct. 2021, Art. no. 127169. [Online]. Available: https://www.sciencedirect.com/science/article/pii/S0030401821004181
[29] D. J. Bogucki, J. A. Domaradzki, R. E. Ecke, and C. R. Truman, "Light scattering on oceanic turbulence," *Appl. Opt.*, vol. 43, no. 30, pp. 5662–5668, 2004.
[30] X. Zhang, M. Lewis, M. Lee, B. Johnson, and G. Korotaev, "The volume scattering function of natural bubble populations," *Limnology Oceanogr.*, vol. 47, no. 5, pp. 1273–1282, Sep. 2002. [Online]. Available:. https://aslopubs.onlinelibrary.wiley.com/doi/abs/10.4319/lo.2002.47.5.1273
[31] H. R. Gordon, "Sensitivity of radiative transfer to small-angle scattering in the ocean: Quantitative assessment," *Appl. Opt.*, vol. 32, no. 36, pp. 7505–7511, 1993.
[32] G. R. Fournier and J. L. Forand, "Analytic phase function for ocean water," *Proc. SPIE*, vol. 2258, pp. 194–202, Oct. 1994.
[33] S. Tang, X. Zhang, and Y. Dong, "Temporal statistics of irradiance in moving turbulent ocean," in *Proc. MTS/IEEE OCEANS*, Bergen, Norway, Jun. 2013, pp. 1–4.
[34] G. C. Mooradian and M. Geller, "Temporal and angular spreading of blue-green pulses in clouds," *Appl. Opt.*, vol. 21, no. 9, pp. 1572–1577, 1982.
[35] Z. Ghassemlooy, W. Popoola, and S. Rajbhandari, *Optical Wireless Communications: System and Channel Modelling With MATLAB*, 1st ed. USA: CRC Press, 2012.
[36] J. G. Proakis and M. Salehi, *Digital Communications*, 5th ed. New York, NY, USA: McGraw-Hill, 2008.
[37] R. A. Shafik, M. S. Rahman, and A. R. Islam, "On the extended relationships among EVM, BER and SNR as performance metrics," in *Proc. Int. Conf. Electr. Comput. Eng.*, Dec. 2006, pp. 408–411.

CALLUM T. GELDARD received the M.Eng. degree in electrical and electronic engineering from Northumbria University, in 2017, and the Ph.D. degree from the Institute of Digital Communications, The University of Edinburgh, in 2021. His Ph.D. project was on underwater optical wireless communication, with a focus on the turbulent underwater channel. His main research interests include underwater optical channel modelling, turbulence mitigation, and optical wireless communications.

JOHN S. THOMPSON (Fellow, IEEE) is currently the Personal Chair of Signal Processing and Communications with the School of Engineering, The University of Edinburgh. He also specializes in antenna array processing, energy-efficient wireless communications, and more recently in the application of machine learning to wireless communications. To date, he has published in excess of 500 journals and conference papers on these topics. In January 2016, he was elevated to a fellow of the IEEE for research contributions to antenna arrays and multi-hop communications. He was also one of four scientists elevated to fellow of the European Association for Signal Processing (EURASIP), in 2023, for "Signal processing advances in multiple antenna and relayed wireless communication systems." He is also an Area Editor of the wireless communications topic in IEEE TRANSACTIONS ON GREEN COMMUNICATIONS AND NETWORKING.

WASIU O. POPOOLA is currently a Professor in communications engineering and the Deputy Director of Learning and Teaching with the School of Engineering, The University of Edinburgh, Edinburgh, U.K. In 2022, he was awarded R.A.Eng./Leverhulme Trust Research Fellowship. He has authored or coauthored more than 150 journal articles/conference papers/patent and several invited articles. He has also coauthored the acclaimed book *Optical Wireless Communications: System and Channel Modeling with MATLAB* and many other book chapters. One of his journal articles ranked No. 2 in terms of the number of full text downloads within IEEE Xplore, in 2008, from the 100's of articles published by *IET Optoelectronics*, since 1980. Another article he has coauthored with one of his Ph.D. students received the Best Poster Award at the 2016 IEEE ICSAE Conference. He is a Science Communicator appearing in science festivals and on "BBC Radio 5live Science" Programme, in October 2017. His primary research interests include digital and optical communications, including VLC/LiFi, FSO, and fiber communications. He is also a fellow of the Institute of Engineering Technology (IET) and Higher Education Academy (HEA). He is an Associate Editor of IEEE ACCESS journal. He was an invited Speaker at various events, including the 2016 IEEE Photonics Society Summer Topicals.